Original Article

MOLECULAR METABOLISM

Empagliflozin activates Wnt/β-catenin to stimulate FUNDC1-dependent mitochondrial quality surveillance against type-3 cardiorenal syndrome

Chen Cai [1,2,4], Feng Wu [1,2,4], Bingjie Zhuang [1,2], Qing Ou [1,2,4], Xiaojie Peng [1,2], Nengxian Shi [1,2], Lan Peng [1,2], Ziying Li [1,2], Jin Wang [3,*], Shumin Cai [1,2,**], Ying Tan [1,2,*]**

ABSTRACT

Objectives: Cardiorenal syndrome type-3 (CRS-3) is an abrupt worsening of cardiac function secondary to acute kidney injury. Mitochondrial dysfunction is a key pathological mechanism of CRS-3, and empagliflozin can improve mitochondrial biology by promoting mitophagy. Here, we assessed the effects of empagliflozin on mitochondrial quality surveillance in a mouse model of CRS-3.

Methods: Cardiomyocyte-specific *FUNDC1*-knockout (FUNDC1^{CKO}) mice were subjected to CRS-3 prior to assessment of mitochondrial homeostasis in the presence or absence of empagliflozin.

Results: CRS-3 model mice exhibited lower heart function, increased inflammatory responses and exacerbated myocardial oxidative stress than sham-operated controls; however, empagliflozin attenuated these alterations. Empagliflozin stabilized the mitochondrial membrane potential, suppressed mitochondrial reactive oxygen species production, increased mitochondrial respiratory complex activity and restored the oxygen consumption rate in cardiomyocytes from CRS-3 model mice. Empagliflozin also normalized the mitochondrial morphology, mitochondrial dynamics and mitochondrial permeability transition pore opening rate in cardiomyocytes. Cardiomyocyte-specific ablation of FUN14 domain-containing protein 1 (*FUNDC1*) in mice abolished the protective effects of empagliflozin on mitochondrial homeostasis and myocardial performance. Empagliflozin activated β-catenin and promoted its nuclear retention, thus increasing FUNDC1-induced mitophagy in heart tissues; however, a β-catenin inhibitor reversed these effects.

Conclusions: In summary, empagliflozin activated Wnt/β-catenin to stimulate FUNDC1-dependent mitochondrial quality surveillance, ultimately improving mitochondrial function and cardiac performance during CRS-3. Thus, empagliflozin could be considered for the clinical management of heart function following acute kidney injury.

Keywords Empagliflozin; Cardiorenal syndrome type-3; FUNDC1; β-catenin; Mitochondria

1. INTRODUCTION

The physiological crosstalk between the heart and the kidneys is necessary to maintain hemodynamic stability, metabolic waste elimination and body function. Cardiorenal syndrome type-3 (CRS-3), also known as acute renocardiac syndrome, is an episode of acute cardiac dysfunction resulting from acute kidney injury (AKI) [1]. The spectrum of CRS-3 includes acute heart failure, acute myocardial infarction, rapid cardiac arrhythmia and acute cardiogenic shock [1]. Although AKI is a recognized pathogenetic factor in CRS-3 that has attracted increasing attention in recent years [2,3], the epidemiology of CRS-3 is still in its infancy. Moreover, the severity of CRS-3 has been largely underestimated, possibly due to a poor understanding of its (patho) physiological mechanisms.

Electron microscopy has been used to observe ultrastructural changes in the myocardium after AKI, and the results have suggested that mitochondrial fragmentation is an initial inducer of cardiomyocyte damage during CRS-3 [4,5]. In addition to mitochondrial morphological

[1]Department of Critical Care Medicine, Nanfang Hospital, Southern Medical University, Guangzhou 510515, China [2]Department of Critical Care Medicine, The First School of Clinical Medicine, Southern Medical University, Guangzhou 510515, China [3]Department of Vascular Medicine, Peking University Shougang Hospital, Beijing 100144, China

[4] These authors contributed equally to this article.

*Corresponding author. Department of Critical Care Medicine, Nanfang Hospital, Southern Medical University, Guangzhou 510515, China. E-mail: tanying0924@163.com (Y. Tan).

**Corresponding author. Department of Critical Care Medicine, Nanfang Hospital, Southern Medical University, Guangzhou 510515, China. E-mail: 13751845166@163.com (S. Cai).

***Corresponding author. Department of Vascular Medicine, Peking University Shougang Hospital, Beijing 100144, China. E-mail: nkuwangjin@163.com (J. Wang).

Received June 15, 2022 • Revision received July 10, 2022 • Accepted July 14, 2022 • Available online 19 July 2022

https://doi.org/10.1016/j.molmet.2022.101553

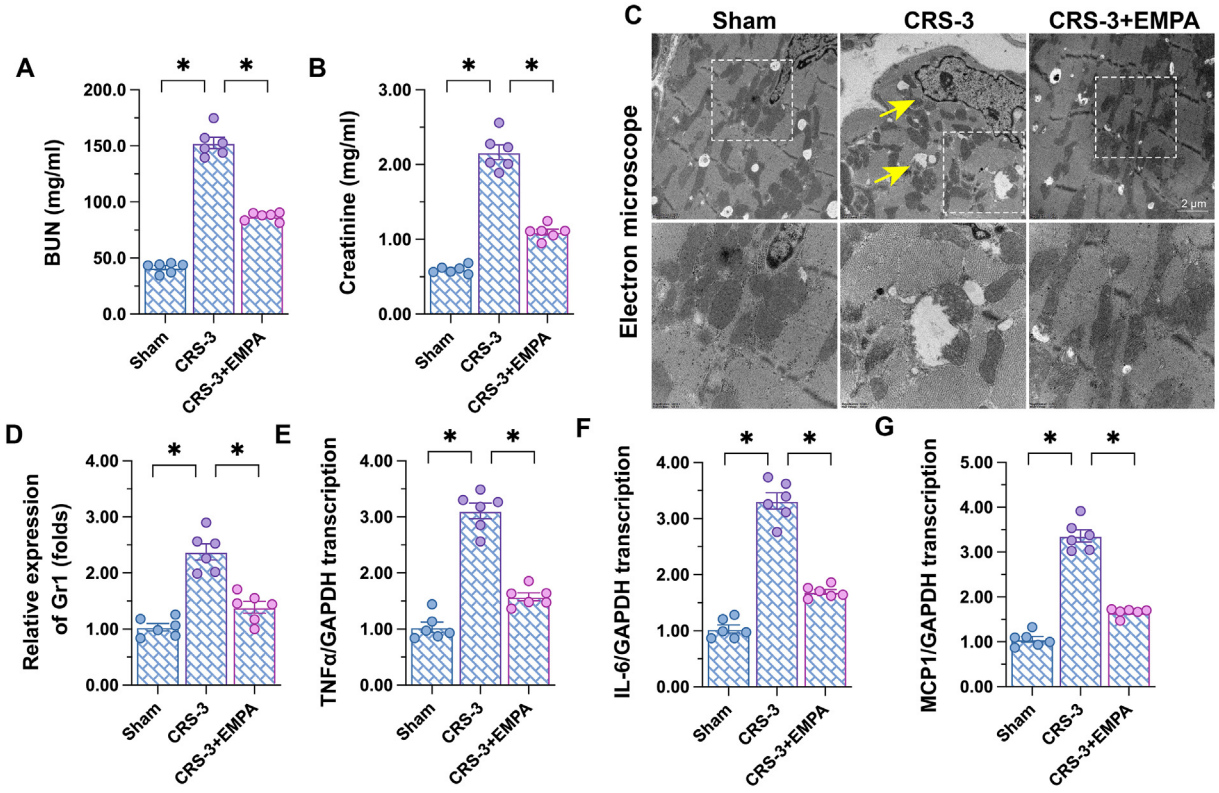

Figure 1: Empagliflozin reduces myocardial damage and improves myocardial function after CRS-3. A WT mouse model of CRS-3 was generated through 30 min of bilateral renal artery ischemia followed by 72 h of reperfusion. Seven days before CRS-3, empagliflozin (EMPA, 10 mg/kg/d) was administered to the mice via oral gavage. **(A, B)** Blood samples were collected from the CRS-3 model mice, and the levels of BUN and creatinine (Cr) were determined using ELISAs. **(C)** Electron microscopy was used to detect changes in the myocardial structure. Yellow arrows indicate myocardial fiber swelling, muscle sarcomere dissolution and mitochondrial vacuolization in response to CRS-3. **(D)** Relative expression of Gr-1 in the myocardium. **(E—G)** RNA was isolated from heart tissues, and qPCR was used to determine the transcription of *IL-6*, *MCP1* and *TNFα*. *$p < 0.05$.

alterations, mitochondrial oxidative stress and the inflammation response have been proposed to reduce cardiomyocyte viability and function during CRS-3 [6]. Attenuated mitochondrial energy metabolism and decreased adenosine triphosphate (ATP) output have also been reported to promote CRS-3 by stimulating myocardial inflammatory responses [7]. A recent study found that the pathogenesis of myocardial damage during CRS-3 involved abnormal mitochondrial calcium signaling due to inositol 1,4,5-trisphosphate receptor/mitochondrial calcium uniporter pathway activation [8]. Based on the above results, we reasoned that perturbed mitochondrial homeostasis could be a key molecular contributor to acute cardiac depression after AKI. FUN14 domain-containing protein 1 (FUNDC1)-dependent mitophagy is an evolutionarily conserved component of the mitochondrial quality surveillance program that repairs dysfunctional mitochondria and maintains mitochondrial homeostasis. Previous research [9—14] have described the protective effects of mitophagy on mitochondrial function and myocardial performance during myocardial ischemia/reperfusion injury or septic cardiomyopathy. However, little is known about the impact of mitophagy on CRS-3. It has been reported that mitophagy is able to reduce mitochondrial oxidative stress, inhibit the inflammation response, block mitochondria-dependent cardiomyocyte apoptosis, reverse mitochondria-involved energy metabolism, enhance mitochondrial antioxidative capacity, promote mitochondrial membrane potential stabilization, and maintain intracellular calcium homeostasis [15—21]. Therefore, it is necessary to figure out whether mitophagy protects against CRS-3.

Table 1 — The difference of echocardiography parameter between mice treated with empagliflozin (EMPA) after acute kidney injury-induced CRS-3.

Parameter	Sham	CRS-3	CRS-3+EMPA
IVSd (mm)	1.09 ± 0.06	1.10 ± 0.07	1.08 ± 0.06
IVSs (mm)	1.25 ± 0.08	1.28 ± 0.07	1.29 ± 0.07
LVIDd (mm)	3.31 ± 0.24	3.28 ± 0.15	3.24 ± 0.20
LVIDs (mm)	2.31 ± 0.17	2.31 ± 0.16	2.27 ± 0.12
LVPWd (mm)	0.89 ± 0.09	0.93 ± 0.08	0.88 ± 0.07
LVPWs (mm)	1.16 ± 0.07	1.15 ± 0.08	1.12 ± 0.06
LVESV(μL)	21.43 ± 2.44	22.24 ± 2.27	22.05 ± 1.79
LVEDV (μL)	48.95 ± 4.67	50.17 ± 5.02	49.86 ± 4.78
LVEF (%)	63 ± 5	44 ± 3#	58 ± 6*
LVFS (%)	32 ± 2	21 ± 3#	29 ± 3*
LVM (mg)	123.15 ± 9.12	151.43 ± 12.78#	132.78 ± 10.42*
E/A	1.35 ± 0.04	0.76 ± 0.04#	1.21 ± 0.08*

LVIDs: left ventricular internal dimension at end systole, LVIDd: left ventricular internal diameter at end diastole, LVESV: left ventricular end systolic volume, LVEDV: left ventricular end diastolic volume, LVPWs: left ventricular posterior wall depth at end systole, LVPWd: left ventricular posterior wall depth at end diastole, IVSs: interventricular septum depth at end systole, IVSd: interventricular septum depth at end diastole, LVEF: left ventricular ejection fraction, LVFS: left ventricular fractional shortening, LVM: left ventricular mass. #$p < 0.05$ vs. Sham, *$p < 0.05$ vs. CRS-3.

Empagliflozin is a novel anti-diabetic drug that reduces glucose reuptake in the proximal tubule. Recent studies [22,23] have identified mitochondria as potential targets of empagliflozin in cardiovascular disorders. Importantly, empagliflozin has exhibited beneficial effects on CRS-1

(acute heart failure-induced AKI) [24] and CRS-4 (chronic kidney disease-induced cardiac abnormalities) [25]. In this study, we sought to determine whether FUNDC1-dependent mitophagy protects the heart against CRS-3, and whether empagliflozin can attenuate CRS-3-associated myocardial depression by improving mitophagic mitochondrial quality surveillance.

2. RESULTS

2.1. Empagliflozin reduces myocardial damage and improves myocardial function after CRS-3

We established a CRS-3 mouse model by subjecting mice to 30 min of bilateral renal artery ischemia followed by 72 h of reperfusion, in accordance with previous study [8,26]. We treated the mice with empagliflozin 7 days before renal reperfusion injury. Mice subjected to a sham operation were used as controls. Then, we analyzed blood urea nitrogen (BUN) and creatinine (Cr) levels to confirm the induction of AKI. Compared with sham-operated mice, CRS-3 model mice exhibited elevated serum concentrations of BUN and Cr, indicating that AKI had been successfully induced (Figure 1A,B).

Next, we assessed heart function in the mice (Table 1). Compared with the sham operation, CRS-3 had little impact on ventricular volume parameters such as the left ventricular internal dimension at end systole (LVIDs), left ventricular internal diameter at end diastole (LVIDd), left ventricular end systolic volume (LVESV), left ventricular end diastolic volume (LVEDV), left ventricular posterior wall depth at end systole (LVPWs), left ventricular posterior wall depth at end diastole (LVPWd), interventricular septum depth at end systole (IVSs) and interventricular septum depth at end diastole (IVSd) (Table 1). However, the left ventricular ejection fraction (LVEF) and left ventricular fractional shortening (LVFS) were impaired in the CRS-3 group compared with the sham group, suggesting that acute renal dysfunction had reduced the systolic capacity (Table 1). Moreover, the E/A value was reduced after CRS-3 compared with the baseline, illustrating that CRS-3 had compromised the diastolic index (Table 1). In CRS-3 model mice treated with empagliflozin, both the systolic capacity and the diastolic parameters of the heart were improved compared with the CRS-3 group (Table 1). In addition, the left ventricular mass (LVM) increased after CRS-3, but returned to near-normal levels in mice treated with empagliflozin, suggesting that empagliflozin can attenuate CRS-3-induced myocardial edema (Table 1). Electron microscopic detection of the myocardial structure demonstrated that CRS-3 induced myocardial fiber swelling, muscle sarcomere dissolution and mitochondrial vacuolization (Figure 1C); however, empagliflozin reversed these phenotypic changes.

Considering that the LVM increased after CRS-3, we wondered whether acute renal dysfunction had induced a myocardial inflammatory response. An immunofluorescence assay revealed that the expression of Gr-1, a marker of neutrophils, was significantly elevated in heart tissues after CRS-3 (Figure 1D). Correspondingly, the mRNA levels of interleukin 6 (*IL-6*), monocyte chemoattractant protein 1 (*MCP1*) and tumor necrosis factor alpha (*TNFα*) were upregulated in heart tissues from CRS-3 model mice (Figure 1E—G). Empagliflozin treatment prevented Gr-1^{+} neutrophil deposition within the myocardium (Figure 1D) and thus repressed pro-inflammatory factor activation (Figure 1E—G) in mice subjected to CRS-3. These results hinted that empagliflozin can alleviate CRS-3-induced heart dysfunction.

2.2. Empagliflozin normalizes the mitochondrial structure in cardiomyocytes during CRS-3

Mitochondrial damage is an important contributor to myocardial dysfunction [18,27]. Thus, we assessed whether empagliflozin sustained myocardial structure and function during CRS-3 by protecting mitochondria. Cardiomyocytes were freshly isolated from mouse hearts after CRS-3, and then immunofluorescence assays were used to observe the mitochondrial structure. In the CRS-3 group, cardiomyocyte mitochondria became small, rounded fragments exhibiting a high degree of fission (Figure 2A—C). The average length of the mitochondria decreased significantly after CRS-3, whereas the number of cardiomyocytes with fragmented mitochondria increased (Figure 2A—C). Empagliflozin treatment maintained the mitochondrial length and reduced the proportion of cardiomyocytes with rounded mitochondria (Figure 2A—C). These findings were confirmed through electron microscopy. Cardiomyocyte mitochondria swelled irregularly, and their cristae became fractured and fuzzy after CRS-3, while these alterations were undetectable in the empagliflozin-treated group (Figure 2D).

At the molecular level, the mitochondrial morphology primarily depends on mitochondrial dynamics, as balanced by fission-related proteins (such as dynamin-related protein 1 [Drp1] and mitochondrial fission 1 protein [Fis1]) and fusion-related factors (such as mitofusin 2 [Mfn2] and optic atrophy 1 [Opa1]) [28,29]. Quantitative PCR (qPCR) analysis illustrated that *Drp1* and *Fis1* mRNA levels were significantly elevated in cardiomyocytes after CRS-3 (Figure 2E—H). In contrast, *Mfn2* and *Opa1* were downregulated in cardiomyocytes following CRS-3 (Figure 2E—H). Empagliflozin supplementation prevented each of these alterations (Figure 2E—H), likely reducing mitochondrial fragmentation in cardiomyocytes.

The mitochondrial permeability transition pore (mPTP) is a physiological pore that regulates substance exchange between the cytoplasm and the mitochondrial matrix [30]. Abnormal mPTP opening is an early hallmark of mitochondria-induced cardiomyocyte death [30]. In the present study, we found that the duration of mPTP opening was significantly extended in cardiomyocytes from the CRS-3 group (Figure 2I—J), which was associated with increased caspase-3 activity (Figure 2K). Empagliflozin treatment prevented mPTP opening (Figure 2I—J) and thus suppressed caspase-3 activation in cardiomyocytes after CRS-3 (Figure 2K). Thus, empagliflozin normalized the mitochondrial structure in cardiomyocytes following CRS-3.

2.3. Empagliflozin attenuates cardiomyocyte mitochondrial dysfunction during CRS-3

We next assessed the influence of empagliflozin on cardiomyocyte mitochondrial function in the presence of CRS-3. The main function of mitochondria is to produce ATP for cellular metabolism. ATP production was significantly reduced in cardiomyocytes after CRS-3, but was normalized upon empagliflozin treatment (Figure 3A). The production of ATP greatly depends on the mitochondrial membrane potential. We found that the mitochondrial membrane potential in cardiomyocytes was lower in the CRS-3 group than in the control group (Figure 3B,C). In cardiomyocytes isolated from CRS-3 model mice, this effect was accompanied by increased production of mitochondrial ROS (Figure 3D,E), a byproduct of mitochondrial oxidative phosphorylation. Empagliflozin treatment stabilized the mitochondrial membrane potential (Figure 3B,C) and thus repressed mitochondrial ROS generation (Figure 3D,E) in cardiomyocytes after CRS-3.

At the molecular level, mitochondrial metabolism is regulated by the mitochondrial respiratory complexes. Enzyme-linked immunosorbent assays (ELISAs) demonstrated that CRS-3 impaired the activities of mitochondrial respiratory complexes I-III in cardiomyocytes, whereas empagliflozin treatment restored them to near-normal levels (Figure 3F—H). CRS-3 also reduced the mitochondrial DNA copy number and transcription in cardiomyocytes (Figure 3I,J), while empagliflozin increased them. Moreover, CRS-3 impaired the baseline

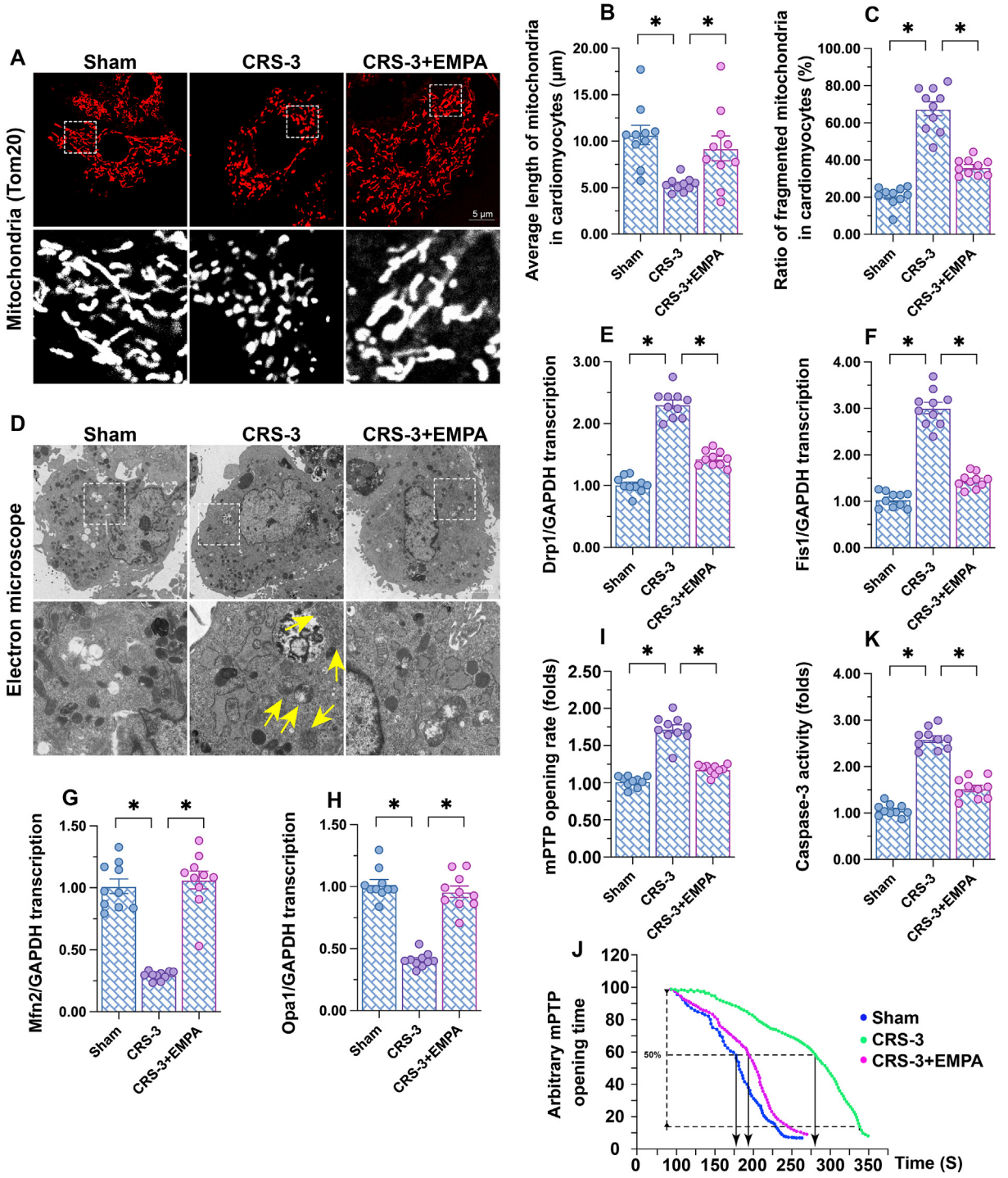

Figure 2: Empagliflozin ameliorates mitochondrial structural disorder in cardiomyocytes during CRS-3. (A–C) Cardiomyocytes were freshly isolated from mouse hearts after CRS-3. Representative pictures of immunofluorescence staining of the mitochondrial morphology are shown. The average mitochondrial length and the number of cardiomyocytes with fragmented mitochondria were recorded. **(D)** Electron microscopy was used to observe the mitochondrial morphology in cardiomyocytes. **(E–H)** RNA was isolated from heart tissues, and qPCR was used to analyze the transcription of *Mfn2*, *Opa1*, *Drp1* and *Fis1*. **(I, J)** The duration of mPTP opening in cardiomyocytes was recorded, and the mPTP opening rate was normalized to that of the control group. **(K)** An ELISA was applied to analyze caspase-3 activity in cardiomyocytes. *$p < 0.05$.

oxygen consumption rate (OCR), proton leak, maximal respiratory capacity and ATP turnover in cardiomyocytes; however, empagliflozin improved the mitochondrial OCR in cardiomyocytes following CRS-3 (Figure 3K-O). These data demonstrated that empagliflozin can improve cardiomyocyte mitochondrial function after CRS-3.

2.4. Empagliflozin activates FUNDC1-dependent mitophagy and preserves mitochondrial integrity in the heart during CRS-3

Mitochondrial damage can be repaired by FUNDC1-dependent mitophagy [12,14]. Therefore, we investigated whether empagliflozin protected cardiomyocyte mitochondria by activating FUNDC1 following

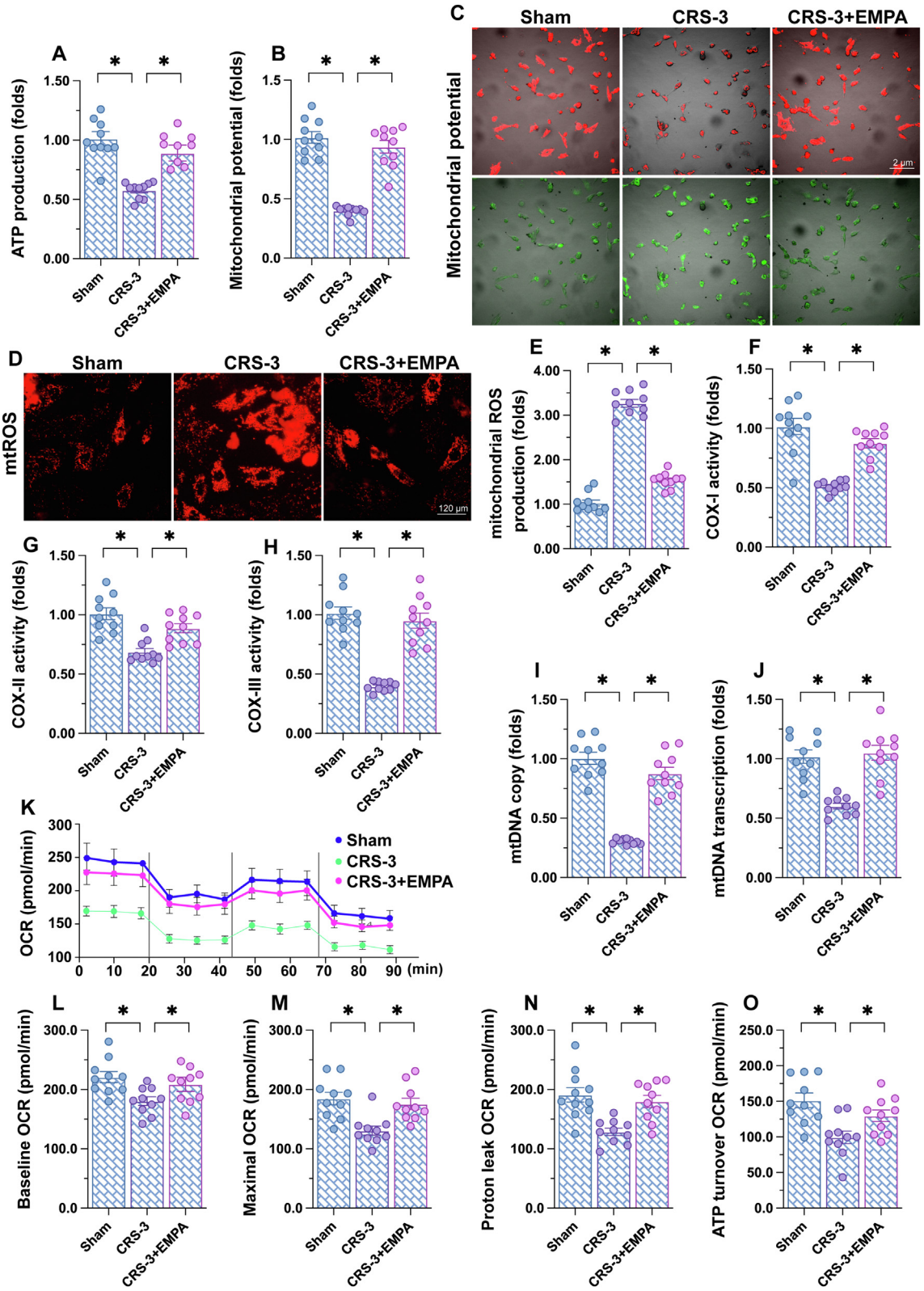

Figure 3: Empagliflozin attenuates cardiomyocyte mitochondrial dysfunction during CRS-3. (A). ATP production in cardiomyocytes was measured with an ELISA. **(B, C)** Representative pictures of the mitochondrial membrane potential analysis using the JC-1 probe. The red-to-green fluorescence ratio was used to quantify the mitochondrial membrane potential in cardiomyocytes. **(D-E)** Representative pictures of the mitochondrial ROS analysis in cardiomyocytes using the MitoSOX red mitochondrial superoxide indicator. **(F—H)** ELISAs were used to observe the changes in mitochondrial respiratory complexes I-III in cardiomyocytes. **(I—J)** The mitochondrial DNA copy number and transcription in cardiomyocytes were determined using qPCR. **(K—O)** The baseline OCR, proton leak, maximal respiratory capacity and ATP turnover in cardiomyocytes were recorded. *$p < 0.05$.

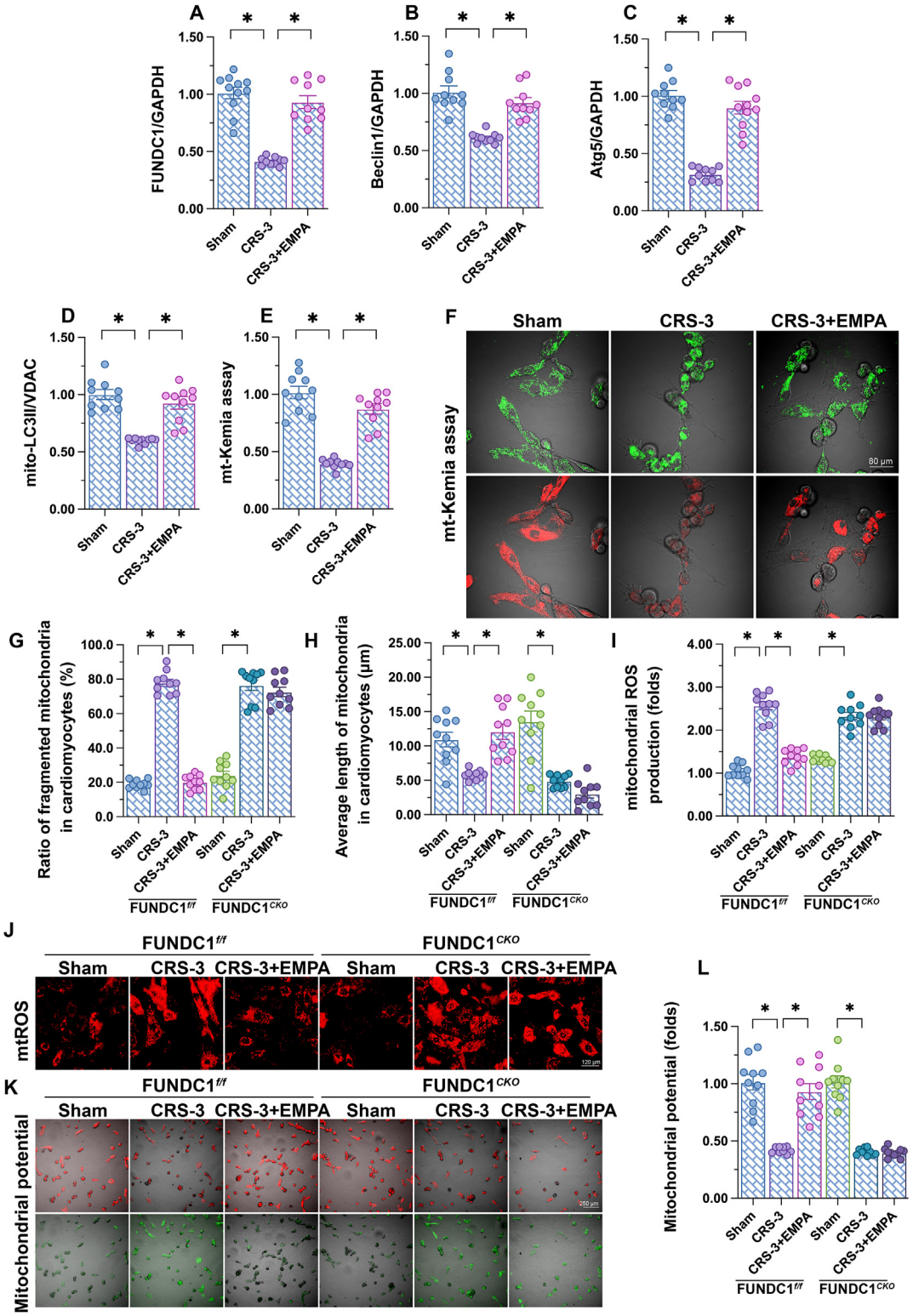

Figure 4: Empagliflozin activates FUNDC1-dependent mitophagy and preserves the mitochondrial integrity in the heart during CRS-3. CRS-3 was induced in cardiomyocyte-specific *FUNDC1* knockout (FUNDC1^{CKO}) mice and control FUNDC1$^{f/f}$ mice. Seven days before CRS-3, empagliflozin (EMPA, 10 mg/kg/d) was administered via oral gavage. Then, cardiomyocytes were isolated from the mice. (**A-D**) Proteins were collected from heart tissues, and FUNDC1, mito-LC3II, Beclin1 and Atg5 protein levels were determined via Western blotting. **(E, F)** Mitophagy activity was measured through an mt-Kemia assay *in vitro*. (**G, H)** Representative pictures of immunofluorescence staining of the mitochondrial morphology in cardiomyocytes. The average mitochondrial length and the number of cardiomyocytes with fragmented mitochondria were recorded. (**I, J)** Representative pictures of the mitochondrial ROS analysis in cardiomyocytes using the MitoSOX red mitochondrial superoxide indicator. (**K, L)** Representative pictures of the mitochondrial membrane potential analysis in cardiomyocytes using the JC-1 probe. The red-to-green fluorescence ratio was used to quantify the mitochondrial membrane potential. *$p < 0.05$.

CRS-3. Western blotting demonstrated that CRS-3 suppressed the expression of FUNDC1 and mitophagy markers such as mitochondrial microtubule-associated protein light chain 3II (mito-LC3II), Beclin1 and autophagy-related gene 5 (Atg5) in heart tissues (Figure 4A—D).

To validate these findings *in vitro*, we used mt-Kemia to analyze the mitophagic flux in cardiomyocytes. When lysosomes enwrap mitochondria, the mitochondrial pH is reduced, and these "acid mitochondria" exhibit red fluorescence upon mt-Kemia staining. Under normal conditions, several dots of red fluorescence were detectable in the cardiomyocytes, indicative of active mitophagy at baseline (Figure 4E,F). In cardiomyocytes exposed to CRS-3, the number of red fluorescent dots was reduced, while empagliflozin reversed this alteration (Figure 4E,F). These results suggested that empagliflozin can restore cardiomyocyte mitophagy in the presence of CRS-3.

To confirm that the mitochondrial protective effects of empagliflozin depended on FUNDC1-induced mitophagy, we used cardiomyocyte-specific *FUNDC1* knockout (FUNDC1^{CKO}) mice. CRS-3 was induced in FUNDC1^{CKO} mice in the presence of empagliflozin, and then cardiomyocytes were isolated from these mice for mitochondrial functional and structural analyses. As shown in Figure 4G—H, cardiomyocytes from FUNDC1^{CKO} mice exhibited a disrupted mitochondrial structure compared with those from control (FUNDC1$^{f/f}$) mice when both groups were subjected to CRS-3 and treated with empagliflozin, as evidenced by shortened mitochondrial lengths and an increased percentage of cells with fragmented mitochondria. Empagliflozin also failed to neutralize mitochondrial ROS production in FUNDC1^{CKO} cardiomyocytes after CRS-3 (Figure 4I,J). Similarly, although empagliflozin sustained the mitochondrial membrane potential in CRS-3-induced cardiomyocytes, the depletion of *FUNDC1* abolished this effect (Figure 4K and L). These results demonstrated that the protective effects of empagliflozin on cardiomyocyte mitochondrial homeostasis depend on FUNDC1-induced mitophagy.

2.5. Loss of FUNDC1 abolishes the cardioprotective effects of empagliflozin during CRS-3

Next, we performed additional experiments to verify that empagliflozin protected the heart against CRS-3 by inducing FUNDC1-dependent mitophagy. Echocardiography illustrated that empagliflozin failed to sustain the LVEF and LVFS in FUNDC1^{CKO} mice compared with FUNDC1$^{f/f}$ mice after CRS-3 (Table 2). Moreover, although empagliflozin normalized the E/A value and LVM following CRS-3, these effects were annulled in FUNDC1^{CKO} mice (Table 2). Regarding myocardial structure, electron microscopy revealed that empagliflozin treatment ameliorated myocardial fiber swelling, muscle sarcomere dissolution and mitochondrial vacuolization after CRS-3 induction in FUNDC1$^{f/f}$ mice, but not in FUNDC1^{CKO} mice (Figure 5A). The deletion of *FUNDC1* also suppressed the anti-inflammatory effects of empagliflozin in heart tissue after CRS-3, as evidenced by increased transcription of *IL-6*, *MCP1* and *TNFα* (Figure 5B—D). These results illustrated that the cardioprotective effects of empagliflozin during CRS-3 largely depend on FUNDC1-induced mitophagy.

2.6. Empagliflozin activates the β-catenin pathway and promotes FUNDC1-dependent mitophagy in cardiomyocytes during CRS-3

Several pathways have been proposed to participate in cardiorenal syndrome, including the Akt [7], β-catenin [31], apoptosis signal-regulating kinase 1 [32], extracellular signal-regulated kinase [33], tumor necrosis factor-like weak inducer of apoptosis [34] and fibronectin type III domain-containing protein 5 pathways [35]. Interestingly, previous studies [36—38] have revealed that the activation and nuclear accumulation of β-catenin can stimulate transcription factor/lymphoid enhancer-binding element transcription factors to induce mitophagy-related genes such as *SQSTM1* (the gene encoding p62) [36,39]. We therefore evaluated whether β-catenin was involved in empagliflozin-induced FUNDC1-dependent mitophagy in CRS-3. β-catenin activity was significantly repressed in heart tissues after CRS-3, as evidenced by increased β-catenin phosphorylation in Western blotting (Figure 6A,B) and reduced nuclear β-catenin expression in immunofluorescence assays (Figure 6C,D). Empagliflozin treatment not only prevented β-catenin phosphorylation (Figure 6A,B), but also restored the abundance of nuclear β-catenin in heart tissues (Figure 6C,D).

We then performed gain- and loss-of-function assays regarding β-catenin. Prior to CRS-3 induction, mice were administered BML-284, an agonist of β-catenin, to simulate the effects of empagliflozin. In contrast, empagliflozin-treated mice were given MSAB, an inhibitor of β-catenin. Then, mitophagy parameters in heart tissues were measured via qPCR. As shown in Figure 6E—G, CRS-3 reduced *FUNDC1*, *p62* and *Beclin1* mRNA levels in heart tissues, while empagliflozin or BML-284 administration restored them to near-

Table 2 — The difference of echocardiography parameter between FUNDC1$^{f/f}$ mice or FUNDC1^{CKO} mice treated with empagliflzoin (EMPA) after acute kidney injury-induced CRS-3.

Parameter	FUNDC1$^{f/f}$ mice			FUNDC1^{CKO} mice		
	Sham	CRS-3	CRS-3+ EMPA	Sham	CRS-3	CRS-3+ EMPA
IVSd (mm)	1.08 ± 0.07	1.09 ± 0.06	1.10 ± 0.08	1.09 ± 0.08	1.10 ± 0.09	1.09 ± 0.07
IVSs (mm)	1.27 ± 0.06	1.25 ± 0.09	1.27 ± 0.08	1.29 ± 0.08	1.26 ± 0.07	1.28 ± 0.07
LVIDd (mm)	3.30 ± 0.26	3.31 ± 0.17	3.29 ± 0.22	3.27 ± 0.26	3.30 ± 0.19	3.27 ± 0.26
LVIDs (mm)	2.31 ± 0.18	2.30 ± 0.17	2.29 ± 0.18	2.26 ± 0.19	2.27 ± 0.21	2.28 ± 0.18
LVPWd (mm)	0.89 ± 0.08	0.91 ± 0.07	0.89 ± 0.09	0.91 ± 0.09	0.88 ± 0.06	0.89 ± 0.10
LVPWs (mm)	1.15 ± 0.07	1.14 ± 0.09	1.14 ± 0.06	1.12 ± 009	1.15 ± 0.07	1.13 ± 0.08
LVESV(μL)	22.13 ± 2.85	23.04 ± 2.76	22.96 ± 2.12	22.77 ± 2.40	22.84 ± 2.31	23.12 ± 2.42
LVEDV (μL)	49.75 ± 5.05	49.35 ± 4.94	50.12 ± 4.87	51.11 ± 4.90	50.24 ± 5.11	50.18 ± 5.32
LVEF (%)	64 ± 6	42 ± 2$^{\#}$	59 ± 6*	65 ± 5	44 ± 3$^{\#\#}$	42 ± 3**
LVFS(%)	33 ± 2	20 ± 3$^{\#}$	30 ± 3*	34 ± 3	21 ± 2$^{\#\#}$	22 ± 3**
LVM(mg)	124.68 ± 10.35	155.47 ± 11.79$^{\#}$	135.24 ± 13.15*	125.78 ± 12.67	158.63 ± 12.11$^{\#\#}$	157.97 ± 10.38**
E/A	1.33 ± 0.05	0.75 ± 0.05$^{\#}$	1.38 ± 0.06*	1.35 ± 0.06	0.77 ± 0.04$^{\#\#}$	0.78 ± 0.05**

LVIDs: left ventricular internal dimension at end systole, LVIDd: left ventricular internal diameter at end diastole, LVESV: left ventricular end systolic volume, LVEDV:left ventricular end diastolic volume, LVPWs: left ventricular posterior wall depth at end systole, LVPWd: left ventricular posterior wall depth at end diastole, IVSs: interventricular septum depth at end systole, IVSd: interventricular septum depth at end diastole, LVEF: left ventricular ejection fraction, LVFS: left ventricular fractional shortening, LVM: left ventricular mass. #p < 0.05 vs. FUNDC1$^{f/f}$ mice in sham group, *p < 0.05 vs. FUNDC1$^{f/f}$ mice in CRS-3 group, ##p < 0.05 vs. FUNDC1^{CKO} mice in sham group, **p < 0.05 vs. FUNDC1$^{f/f}$ mice in CRS-3+EMPA group.

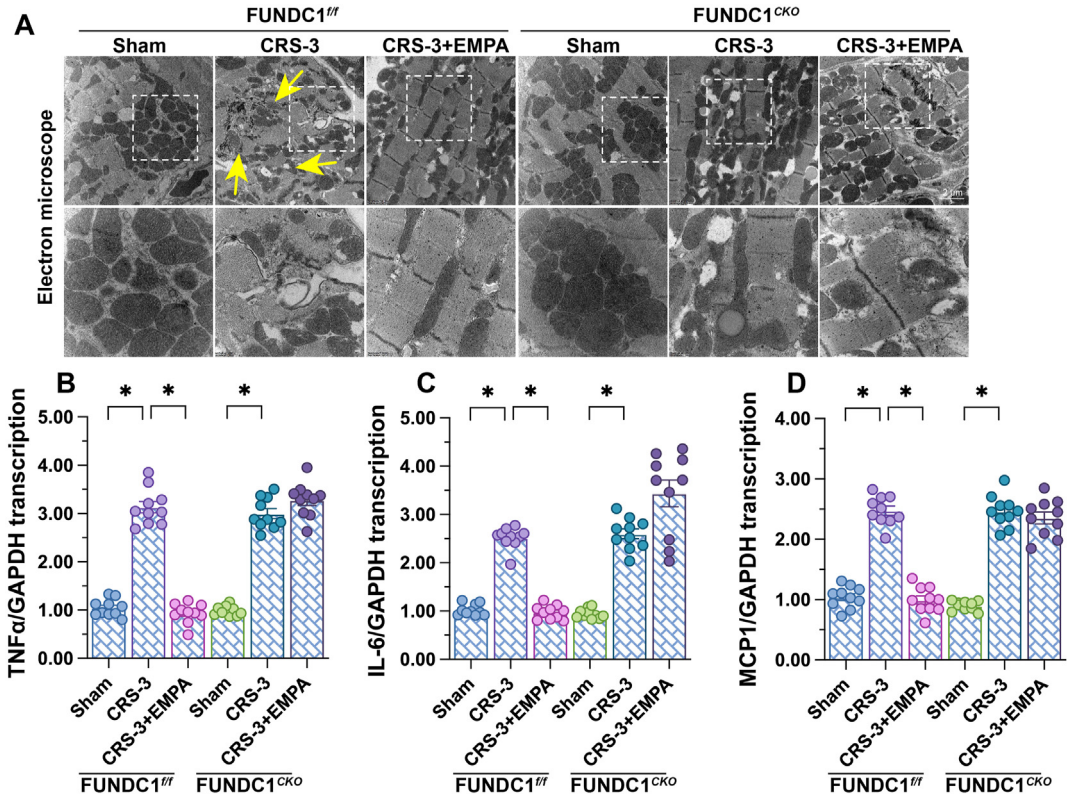

Figure 5: Loss of *FUNDC1* abolishes the cardioprotective effects of empagliflozin during CRS-3. CRS-3 was induced in cardiomyocyte-specific *FUNDC1* knockout (FUNDC1^{CKO}) mice and control FUNDC1$^{f/f}$ mice. Seven days before CRS-3, empagliflozin (EMPA, 10 mg/kg/d) was administered via oral gavage. **(A)** Electron microscopy was used to detect changes in the myocardial structure. Yellow arrows indicate myocardial fiber swelling, muscle sarcomere dissolution and mitochondrial vacuolization in response to CRS-3. (**B**–**D**) RNA was isolated from heart tissues, and qPCR was used to determine the transcription of *IL-6*, *MCP1* and *TNFα*. *$p < 0.05$.

normal levels. MSAB abolished these beneficial effects of empagliflozin in heart tissues following CRS-3 (Figure 6E–G). These findings were further supported by mt-Kemia assays *in vitro*. CRS-3 inhibited mitophagy in cardiomyocytes, and empagliflozin or BML-284 restored it, while MSAB blocked empagliflozin-induced mitophagy activation (Figure 6H,I). These results illustrated that empagliflozin restores mitophagy in cardiomyocytes following CRS-3 by directly activating β-catenin.

3. DISCUSSION

CRS-3 is characterized by abrupt myocardial depression due to acute kidney dysfunction. To date, there is no effective drug to prevent this cardiac malfunction, and the evidence-based therapy in clinical practice is renal replacement therapy. In the present study, we found that empagliflozin could attenuate myocardial damage during CRS-3 by activating β-catenin and inducing FUNDC1-dependent mitophagy, thus protecting mitochondrial function and preserving cardiac performance. The primary findings of our study are as follows: 1) empagliflozin improved cardiomyocyte structure, maintained heart systolic and diastolic function, alleviated myocardial inflammation and neutralized oxidative injury in the context of CRS-3; 2) empagliflozin prevented mitochondrial morphological disorder and abnormal mPTP opening in cardiomyocytes following CRS-3; 3) empagliflozin sustained cardiomyocyte mitochondrial function during CRS-3, including ATP synthesis, ROS production and oxygen consumption; 4) in molecular experiments, empagliflozin improved mitochondrial structure and function by activating FUNDC1-dependent mitophagy in cardiomyocytes after CRS-3; 5) *in vitro* and *in vivo,* ablation of *FUNDC1* abolished the protective effects of empagliflozin on mitochondrial structure/function and heart performance in response to CRS-3 stress; 6) empagliflozin activated β-catenin by preventing its phosphorylation and cytoplasmic retention in cardiomyocytes following CRS-3, thus transcriptionally activating FUNDC1-dependent mitophagy. Our study is the first to describe the therapeutic mechanisms and effects of empagliflozin during CRS-3, and suggests that drugs designed to alter the β-catenin/FUNDC1/mitophagy/mitochondrial quality surveillance pathway could be developed to treat CRS-3.

Several pathological alterations in the myocardium have been observed during CRS-3, including oxidative stress, inflammation, mild cardiomyocyte apoptosis, catecholamine accumulation, metabolic reprogramming, intracellular calcium reuptake disorder, mitochondrial dysfunction and endoplasmic reticulum stress [6,7,10,40,41]. Among these pathological inducers, impaired mitochondrial quality seems to drive the other pathological processes that aggravate myocardial damage during CRS-3 [7,42]. The number of mitochondria is higher in cardiomyocytes than in many other types of cells, including skeletal muscle cells, endothelial cells, hepatocytes and renal tubular cells [43]. Mitochondria consume oxygen and produce ATP to support cardiomyocyte contraction and relaxation. Therefore, mitochondrial damage is inevitably followed by compromised cardiomyocyte metabolism, which features amino acid depletion and a metabolic shift from oxidative phosphorylation to anaerobic forms of energy production during CRS-3 [44]. Moreover, because mitochondrial damage impairs

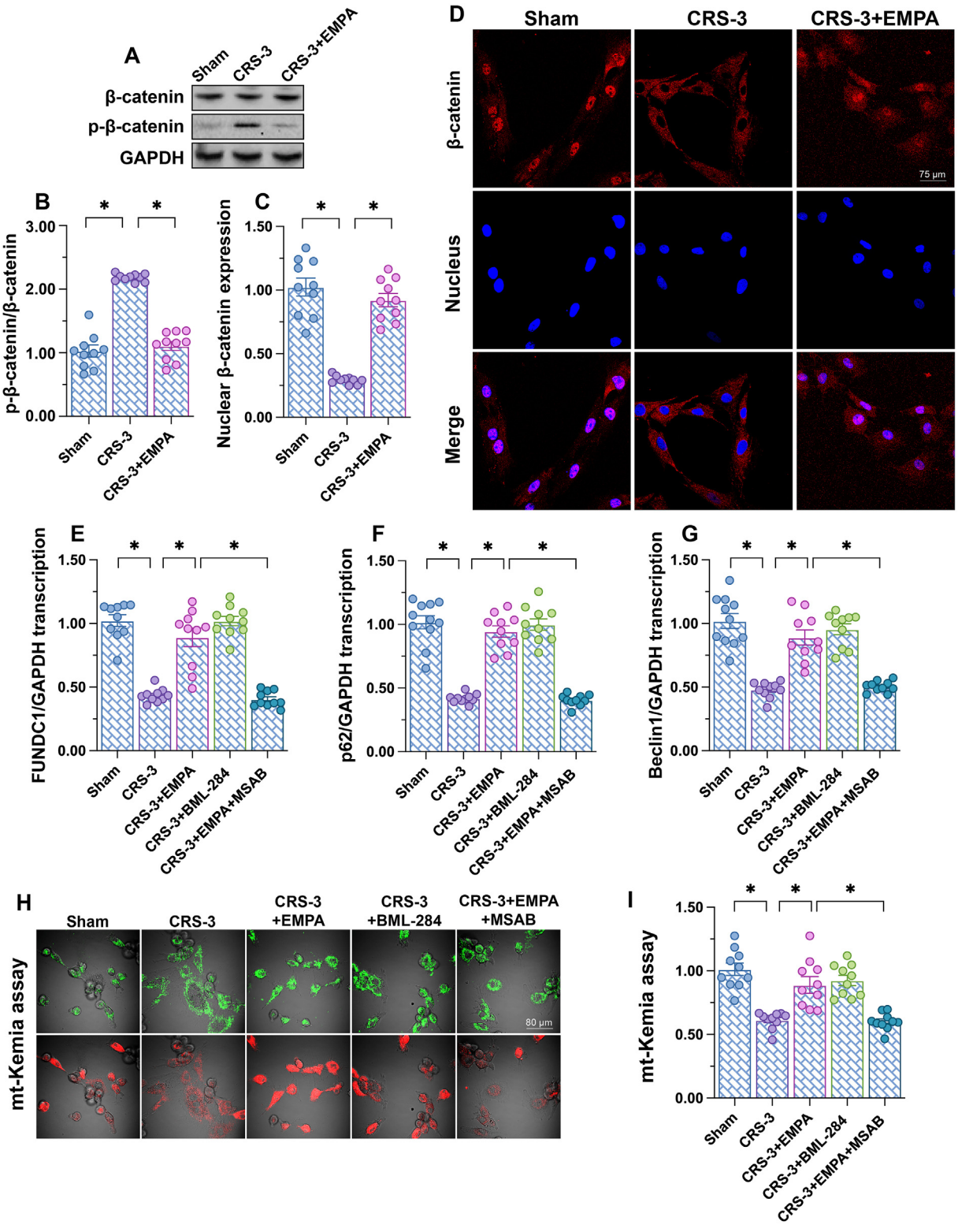

Figure 6: Empagliflozin activates the β-catenin pathway and promotes FUNDC1-dependent mitophagy in cardiomyocytes during CRS-3. A WT mouse model of CRS-3 was generated through 30 min of bilateral renal artery ischemia followed by 72 h of reperfusion. Seven days before CRS-3, empagliflozin (EMPA, 10 mg/kg/d) was administered via oral gavage. To activate or inhibit the Wnt/β-catenin pathway, mice were respectively treated with BML-284 (5 mg/kg) or MSAB (10 mg/kg) two days before CRS-3 or empagliflozin treatment. **(A, B)** Proteins were collected from heart tissues, and β-catenin expression was determined using Western blotting. **(C, D)** Representative pictures of immunofluorescence staining with a β-catenin antibody. Nuclei were stained with DAPI. The levels of nuclear β-catenin were determined. **(E–G)** RNA was isolated from heart tissues, and qPCR was used to determine the transcription of *FUNDC1*, *p62* and *Beclin1*. **(H, I)** Mitophagy activity was measured through an mt-Kemia assay *in vitro*. *$p < 0.05$.

mitochondrial respiration and mitochondrial anti-oxidative enzyme activity, oxidative stress is a direct byproduct of mitochondrial damage in cardiomyocytes during CRS-3 [45]. Reduced ATP production or increased oxidative stress in mitochondria upregulates calcium-releasing channels such as the inositol 1,4,5-trisphosphate receptor [8] and suppresses the activity of calcium-reuptake proteins such as sarcoplasmic/endoplasmic reticulum calcium ATPase 2a [46]. This leads to a systolic calcium deficit and/or diastolic calcium leak, which increases the likelihood of arrhythmogenic events and reduces the cardiac contractile capacity [47]. Ultimately, unhealthy mitochondria induce cell death by activating caspase-3/7/9 in cardiomyocytes during CRS-3 [48]. Of note, cell death inherently provokes the inflammatory response, which may cause a chain reaction that exacerbates cardiomyocyte damage during CRS-3 [7]. Consistent with these observations, we found that both mitochondrial function and structure were disrupted in cardiomyocytes during CRS-3. However, protecting mitochondrial homeostasis through empagliflozin supplementation sustained cardiac performance, confirming that mitochondrial damage promotes the pathology of CRS-3 through multiple distinct signaling cascades and molecular events.

There is ample evidence that empagliflozin is beneficial to mitochondria in various disease models. In myocardia isolated from patients with heart failure with preserved ejection fraction, empagliflozin suppressed the levels of mitochondrial oxidative parameters such as hydrogen peroxide, 3-nitrotyrosine, glutathione and lipid peroxides [49]. In type-1 diabetes patients, empagliflozin increased lipid and tricarboxylic acid cycle metabolites [50], suggesting that this treatment shifted metabolic substrate use and improved mitochondrial function. A transcriptomic analysis in a mouse model of nonalcoholic fatty liver disease revealed that empagliflozin enhanced mitochondrial triglyceride transfer, triglyceride lipolysis and β-oxidation [51]. In ethanol-induced cardiomyopathy, empagliflozin reduced mitochondria-induced apoptosis in cardiomyocytes by normalizing the Bcl-2/Bax ratio [52]. In addition to ameliorating chronic diseases, empagliflozin was found to enhance mitochondrial biogenesis in a rat model of acute ischemia/reperfusion injury by upregulating nuclear factor erythroid 2-related factor 2 and peroxisome proliferator-activated receptor gamma coactivator 1-alpha [53]. Pretreatment with empagliflozin partly improved heart function, reduced serum cardiac troponin I levels, increased myocardial ketone levels and maintained the mitochondrial ultrastructural integrity after cardiac arrest [54]. In accordance with the above findings, we found that empagliflozin enhanced many aspects of mitochondrial biology in cardiomyocytes during CRS-3, including the mitochondrial membrane potential, mitochondrial ROS production, mitochondrial respiration, mitochondrial dynamics and mitochondria-induced cell apoptosis.

In the present study, the protective effects of empagliflozin on mitochondria could be explained by the induction of mitophagy, an endogenous repair mechanism for mitochondrial damage. In fact, previous studies have identified mitophagy as a potential target of empagliflozin [55,56]. In a rat model of type-2 diabetes, empagliflozin restored BCL2 interacting protein 3-induced mitophagy and thus reduced mitochondrial fragmentation in the heart [57]. Similarly, empagliflozin activated FUNDC1-dependent mitophagy through the adenosine monophosphate-activated protein kinase/Unc-51-like autophagy-activating kinase 1 pathway in endothelial cells during cardiac ischemia/reperfusion injury [56]. Interestingly, FUNDC1-dependent mitophagy has been recognized as a key protector against myocardial injury during CRS-3 [10]. In FUNDC1^{CKO} mice subjected to CRS-3, we found that empagliflozin failed to protect mitochondrial function/structure and myocardial performance. Nevertheless, the mechanism whereby empagliflozin activated FUNDC1-dependent mitophagy and improved mitochondrial homeostasis remained unclear. Further analyses of heart tissues revealed that empagliflozin activated the Wnt/β-catenin pathway, a transcriptional promoter of mitophagy-related gene expression [36,39]. Accordingly, the inhibition of β-catenin prevented empagliflozin from inducing FUNDC1-dependent mitophagy in cardiomyocytes following CRS-3.

Overall, by using genetic deletion and biochemical approaches *in vitro* and *in vivo*, we have shown for the first time that empagliflozin activates β-catenin to improve mitochondrial quality surveillance through FUNDC1-dependent mitophagy in cardiomyocytes, thus preserving myocardial function during CRS-3. These findings illustrate the multiple effects of empagliflozin on cardiomyocyte mitochondria, and may facilitate the development of therapies to treat CRS-3.

4. MATERIALS AND METHODS

4.1. Mice and induction of CRS-3

Cardiomyocyte-specific *FUNDC1* knockout (FUNDC1^{CKO}) mice were established as we previously described [12]. FUNDC1$^{f/f}$ mice were used as the control group for FUNDC1^{CKO} mice. The CRS-3 model was established as we previously described [8]. Briefly, wild-type (WT) or FUNDC1^{CKO} littermates (10 weeks old) were anesthetized with 2—3.5% isoflurane and maintained at 0.6—1.0% isoflurane. Then, AKI was induced through 30 min of bilateral renal artery ischemia followed by 72 h of reperfusion. Seven days before CRS-3, empagliflozin (10 mg/kg/d) was administered to the mice via oral gavage with 0.5% hydroxyethylcellulose as the vehicle, based on previous findings. Empagliflozin was kindly provided by Boehringer Ingelheim Pharma GmbH & Co. KG, Germany. For Wnt/β-catenin pathway activation or inhibition, mice respectively received BML-284 (5 mg/kg, Selleck, Cat. S8178) or MSAB (10 mg/kg, Cat. S6901) two days before CRS-3 or empagliflozin treatment.

4.2. Echocardiographic/ultrasonographic measurements

Trans-thoracic aortic and cardiac echocardiography/ultrasonography was performed on mice via a Vevo 2100 instrument with an MS400 linear array transducer (Fujifilm Visualsonics) at 18—38 MHz, as previously described. A single trained echocardiographer (N.G.Z.T.) blinded to the genotypes and treatment groups conducted the experiments. Mice were anesthetized with 2—3.5% isoflurane and maintained at 0.6—1.0% isoflurane, while their body temperature was maintained at 37 °C on a heated platform. Their chest and neck hair was removed using a depilatory cream, and a layer of acoustic coupling gel was applied to their thorax. The diameters of the aortic root (Ao Root) and ascending aorta (Asc Ao) were assessed from B and M-mode of the parasternal long-axis view using the inner edge-to-inner edge method, in accordance with the widely accepted American and European guidelines. Aortic parameters were indexed to body weight to account for temporal changes and gender differences in body weight. The peak aortic flow velocity was obtained through the application of a pulsed-wave Doppler across the aortic valve from the aortic arch in suprasternal view. All measurements were averaged over three cardiac cycles.

4.3. Cardiomyocyte isolation and culture

Mice were injected with pentobarbital (120 mg/kg) as a terminal procedure, and their hearts were removed via bilateral thoracotomy. The hearts were immediately plunged into ice-cold Tyrode's solution and mounted on a Langendorff apparatus before undergoing

retrograde perfusion through the aorta with Tyrode's solution (140 mM NaCl, 5.4 mM KCl, 1 mM $CaCl_2$, 1 mM $MgCl_2$, 10 mM HEPES, 5.6 mM glucose, pH 7.3) containing collagenase II (Worthington Biochemical Corp., Lakewood, NJ, USA) at 37 °C for 20 min [58]. The ventricles were minced and placed in a 37 °C water bath shaker in collagenase solution. Isolated cardiomyocytes were plated onto laminin-coated glass coverslips in 24-well plates containing serum-free medium 199 (Thermo Fisher Scientific) supplemented with 25 mmol/L $NaHCO_3$, 10 mmol/L HEPES, 5 mmol/L creatine, 5 mmol/L taurine, 10 μg/mL penicillin, 10 μg/mL streptomycin and 10 μg/mL gentamycin. Cardiomyocytes were cultured at 37 °C in 95% air, 5% CO_2 for at least 36 h before analysis.

4.4. OCR assays

The cellular OCR was measured using a Seahorse XFe 96 Extracellular Flux Analyzer (Seahorse Bioscience) in accordance with our previous studies [13,59]. Experiments were performed according to the manufacturer's instructions. The OCR was measured using a Seahorse XF Cell Mito Stress Test Kit (Agilent Technologies, CA, USA). Briefly, cells were isolated from heart tissues after CRS-3 with or without empagliflozin treatment. After the cells were harvested, the cell number was counted [60]. Ten thousand cells per well were then seeded into a Seahorse XF 96-cell culture microplate for 10 h, at which time the cell number for each group was very similar. The cells were subsequently used for OCR measurements. After baseline measurements of the OCR, the following compounds were sequentially injected: oligomycin, p-trifluoromethoxy carbonyl cyanide phenylhydrazone (FCCP, a reversible inhibitor of oxidative phosphorylation), and the mitochondrial complex I inhibitor rotenone plus the mitochondrial complex III inhibitor antimycin A (Rote/AA). Data were analyzed using Seahorse XF-96 Wave software, and the results were normalized to the cell number. The OCR is reported in pmol/min.

4.5. ROS assay

Mitochondrial ROS emission within the mitochondrial matrix in cardiomyocytes was assessed using the MitoSOX red mitochondrial superoxide indicator (Molecular Probes, USA), as we described previously. The probe was excited using 405 nm and 488 nm laser lines, and fluorescence emission was collected at 520—540 nm wavelengths, measured in the x-y mode at a sampling rate of 400 Hz. Minimum fluorescence was obtained through the application of dithiothreitol (5 mmol/L), and maximum fluorescence (Fmax) was obtained through the application of DTDP (200 μmol/L) [61]. Data are presented as a percentage of $\Delta F/\Delta Fmax$, where $\Delta F = F\text{-}Fmin$ and $\Delta Fmax = Fmax\text{-}Fmin$.

ROS levels in heart tissues were estimated using the ROS probe DHE (Beyotime Institute of Biotechnology, Shanghai, China) according to the manufacturer's instructions. Briefly, heart tissues were washed with cold phosphate-buffered saline and then treated with 10 μM DHE. After the tissues were incubated for 30 min at 37 °C in the dark, the fluorescence intensity was measured with a flow cytometer or fluorescence microplate reader (excitation: 488 nm; emission: 525 nm). Data were analyzed using FlowJo software or GraphPad Prism 8.0.

4.6. Immunofluorescence staining

Cells were grown on four-well microscopic slides for 48 h (24 h in medium with 10% serum and 24 h in medium without serum). Cells or heart tissues were washed in PBS and fixed with 4% PFA at room temperature for 20 min followed by permeabilization with 0.3% Triton X-100 in PBS for 5 min [62]. The fixed samples were blocked with 5% normal goat or donkey serum in PBS for 1 h at room temperature. Primary antibodies against translocase of outer mitochondrial membrane 20 (Tom-20; 1:500, Abcam, #ab78547), Gr-1 (1:500, Abcam, #ab25377) and troponin T (1:500, Abcam, #ab8295) were used. Indirect fluorescent detection was conducted using goat anti-rabbit or goat anti-mouse secondary antibodies conjugated with Alexa Fluor dyes (Invitrogen/Life Technologies). Nuclei were stained with 4′,6-diamidino-2-phenylindole (DAPI), and coverslips were placed. The stained slides were examined under a Zeiss Axio Observer with Apotome. Mitophagy was determined using mt-Kemia, as we previously described.

4.7. ELISA and biochemical analyses

Cell pellets were collected after each treatment. ELISA quantifications of caspase-3 activity (Mouse Caspase-3 ELISA kit, cat. no. MBS733100, MyBioSource), serum BUN (BUN ELISA kit, cat. no. MBS751125, MyBioSource) and serum creatinine (Creatinine ELISA kit, cat. no. MBS2540563, MyBioSource) were performed as per the manufacturer's instructions. Intracellular ATP production was assessed using a commercial kit (ATP/Adenosine Triphosphate ELISA kit, cat. no. LS-F24998, LifeSpan BioSciences, USA) according to the manufacturer's instructions.

4.8. Mitochondrial membrane potential and mPTP opening rate detection

The mitochondrial membrane potential was measured using an MMP assay kit (Solarbio, Beijing, China). Cells were stained with the unique fluorescent probe JC-10 at 37 °C for 20 min, and then were washed twice with phosphate-buffered saline [63]. The fluorescence intensity of the cells was observed using a flow cytometer (BD FACSCalibur, NJ, USA) and a confocal laser scanning microscope (Olympus, Japan). Then, the average fluorescence intensity of green monomers and red aggregates was determined, and the ratio was calculated. To track mPTP opening, we treated cardiomyocytes with tetramethylrhodamine ethyl ester, based on our previous research [12,64]. The fluorescent signal of tetramethylrhodamine ethyl ester was determined using a Nikon confocal microscope system and camera.

4.9. qPCR assay

Total RNA was extracted from heart tissues or harvested cardiomyocytes using TRIzol Reagent. The RNA was dissolved to 500 ng/μL in diethyl pyrocarbonate-treated water. Real-time qPCR was performed using SYBR Green PCR Master Mix (Q311-02, ChamQ SYBR qPCR Master Mix, Vazyme) according to the manufacturer's protocol [65]. The comparative Ct method was used to determine gene expression relative to the housekeeping gene b-actin (*ACTB*), and the results were expressed as relative mRNA levels compared with the internal control (α-tubulin). The following primer pairs were used: *TNFα* (Forward, 5′- AGATGGAGCAACCTAAGGTC-3'; Reverse, 5′-GCAGACCTCGCTGTTCTAGC-3′), *IL-6* (Forward, 5′-CAGACTCGCGCCTCTAAGGAGT-3'; Reverse, 5′-GATAGCCGATCCGTCGAA-3′), *MCP1* (Forward, 5′-GGATGGATTGCACAGCCATT-3'; Reverse, 5′-GCGCCGACTCAGAGGTGT-3′), *GAPDH* (Forward, 5′-TCGATATTGAGCGTCCAACCT-3′; Reverse, 5′-CAAAGGCACGTTTGGCATACA-3′), *Drp1* (Forward, 5′-GGGCACTTAAATTGGGCTCC-3'; Reverse, 5′-TGTATTCTGTTGGCGTGGAAC-3′), *Fis1* (Forward, 5′-GGCTGTCTCCAAGTCCAAATC-3′; Reverse, 5′-GGAGAAAAGGGAAGGCGATG-3′), *Opa1* (Forward, 5′-TCACCTCTGCGTTTATTTGAAGA-3′; Reverse, 5′-GGGTAGAACGGGAGGAAAGG-3′), *Mfn2* (Forward, 5′-GGAGACCAACAAGGACTGGA-3′; Reverse, 5′-TGCACAGTGACTTTCAACCG-3′), *p62* (Forward, 5′-GAGGCACCCCGAAACATGG-3'; Reverse, 5′-ACTTATAGCGAGTTCCCACCA-3′) and *Beclin1* (Forward, 5′-ATGGAGGGGTCTAAGGCGTC-3'; Reverse, 5′-TCCTCTCCTGAGTTAGCCTCT-3′).

4.10. Western blot analysis

Heart tissues or cardiomyocytes were homogenized with radioimmunoprecipitation assay buffer containing phenylmethylsulfonyl fluoride and a phosphatase inhibitor for 30 min. After the samples were centrifuged at 12,000$\times g$ for 30 min, the supernatants were collected for analysis of the protein concentrations [66]. The protein samples were then subjected to 10% or 12% sodium dodecyl sulfate polyacrylamide gel electrophoresis and transferred onto a polyvinylidene difluoride membrane (IPVH00010; Millipore, Billerica, MA, USA). The proteins on the membrane were immunolabeled with primary antibodies at 4 °C overnight, and then were incubated with the corresponding secondary antibodies for two hours at room temperature. The signals were detected with a chemiluminescence imaging system (Bio-Rad, Hercules, CA, USA). The following primary antibodies from Abcam were used at a 1:1000 dilution: β-catenin (#ab184919), p-β-catenin (#ab75777), FUNDC1 (#ab224722), Atg5 (#ab108327), Beclin1 (#ab207612), p62 (#ab91526) and LC3II (#ab192890).

4.11. Statistical analyses

All samples or animals were assigned randomly to their groups, and the experiments were performed in a blinded fashion. All data are presented as the mean ± standard deviation. The analyses were performed with SPSS software version 21.0. The variation estimate of the data was obtained, and its normal distribution was then confirmed. Differences between two groups were tested using Student's t-test. Comparisons among multiple groups were performed using one-way analysis of variance. Bonferroni's *post hoc* test was used when the variances were homogeneous, and Tamhane's T2(M) *post hoc* test was used otherwise. P values < 0.05 were considered statistically significant.

FUNDING

This study is supported by the National Natural Science Foundation of China (NO. 82102262), the Guangdong Basic and Applied Basic Research Foundation (NO. 2021A1515010977 and NO. 2020A1515110174).

AUTHORS' CONTRIBUTIONS

Chen Cai, Jin Wang, Feng Wu, and Bingjie Zhuang conceived the original experiments. Qing Ou, Xiaojie Peng, Nengxian Shi, and Lan Peng carried out all the *in vivo* experiments and molecular investigation *in vitro*. Ying Tan, Ziying Li and Shumin Cai wrote the whole manuscript. Ying Tan revised the final version of manuscript. All the authors read the article and approved the submission.

ACKNOWLEDGMENTS

None.

CONFLICT OF INTEREST

The authors have declared that they have no conflicts of interest.

REFERENCES

[1] Rangaswami, J., Bhalla, V., Blair, J.E.A., Chang, T.I., Costa, S., Lentine, K.L., et al., 2019. Cardiorenal syndrome: classification, pathophysiology, diagnosis, and treatment strategies: a scientific statement from the American heart association. Circulation 139(16):e840—e878.

[2] Chuasuwan, A., Kellum, J.A., 2012. Cardio-renal syndrome type 3: epidemiology, pathophysiology, and treatment. Seminars in Nephrology 32(1):31—39.

[3] Wang, J., Zhang, W., Wu, L., Mei, Y., Cui, S., Feng, Z., et al., 2020. New insights into the pathophysiological mechanisms underlying cardiorenal syndrome. Aging (Albany NY) 12(12):12422—12431.

[4] Sumida, M., Doi, K., Ogasawara, E., Yamashita, T., Hamasaki, Y., Kariya, T., et al., 2015. Regulation of mitochondrial dynamics by dynamin-related protein-1 in acute cardiorenal syndrome. Journal of the American Society of Nephrology 26(10):2378—2387.

[5] Doi, K., Noiri, E., 2016. Mitochondrial dysfunction in cardiorenal syndrome. Antioxidants and Redox Signaling 25(4):200—207.

[6] Neres-Santos, R.S., Junho, C.V.C., Panico, K., Caio-Silva, W., Pieretti, J.C., Tamashiro, J.A., et al., 2021. Mitochondrial dysfunction in cardiorenal syndrome 3: renocardiac effect of vitamin C. Cells 10(11).

[7] Wang, J., Sun, X., Wang, X., Cui, S., Liu, R., Liu, J., et al., 2021. Grb2 induces cardiorenal syndrome type 3: roles of IL-6, cardiomyocyte bioenergetics, and akt/mTOR pathway. Frontiers in Cell and Developmental Biology 9:630412.

[8] Wang, J., Toan, S., Li, R., Zhou, H., 2020. Melatonin fine-tunes intracellular calcium signals and eliminates myocardial damage through the IP3R/MCU pathways in cardiorenal syndrome type 3. Biochemical Pharmacology 174:113832.

[9] Ji, H., Wang, J., Muid, D., Song, W., Jiang, Y., Zhou, H., 2022. FUNDC1 activates the mitochondrial unfolded protein response to preserve mitochondrial quality control in cardiac ischemia/reperfusion injury. Cellular Signalling 92:110249.

[10] Wang, J., Wang, X., Du, W., Xue, Z., Huang, W., Guan, Z., et al., 2022. BI-1 ameliorates myocardial injury by activating the mitochondrial unfolded protein response and FUNDC1-related mitophagy in cardiorenal syndrome type 3. Cellular Signalling 91:110218.

[11] Zhang, W., 2021. The mitophagy receptor FUN14 domain-containing 1 (FUNDC1): a promising biomarker and potential therapeutic target of human diseases. Genes Dis 8(5):640—654.

[12] Zhou, H., Zhu, P., Wang, J., Zhu, H., Ren, J., Chen, Y., 2018. Pathogenesis of cardiac ischemia reperfusion injury is associated with CK2alpha-disturbed mitochondrial homeostasis via suppression of FUNDC1-related mitophagy. Cell Death & Differentiation 25(6):1080—1093.

[13] Zhou, H., Wang, J., Zhu, P., Zhu, H., Toan, S., Hu, S., et al., 2018. NR4A1 aggravates the cardiac microvascular ischemia reperfusion injury through suppressing FUNDC1-mediated mitophagy and promoting Mff-required mitochondrial fission by CK2alpha. Basic Research in Cardiology 113(4):23.

[14] Wang, J., Zhu, P., Li, R., Ren, J., Zhou, H., 2020. Fundc1-dependent mitophagy is obligatory to ischemic preconditioning-conferred renoprotection in ischemic AKI via suppression of Drp1-mediated mitochondrial fission. Redox Biology 30:101415.

[15] Wang, S., Zhu, H., Li, R., Mui, D., Toan, S., Chang, X., et al., 2022. DNA-PKcs interacts with and phosphorylates Fis1 to induce mitochondrial fragmentation in tubular cells during acute kidney injury. Science Signaling 15(725):eabh1121.

[16] Zhu, H., Toan, S., Mui, D., Zhou, H., 2021. Mitochondrial quality surveillance as a therapeutic target in myocardial infarction. Acta Physiologica 231(3):e13590.

[17] Zhu, H., Tan, Y., Du, W., Li, Y., Toan, S., Mui, D., et al., 2021. Phosphoglycerate mutase 5 exacerbates cardiac ischemia-reperfusion injury through disrupting mitochondrial quality control. Redox Biology 38:101777.

[18] Zhou, H., Ren, J., Toan, S., Mui, D., 2021. Role of mitochondrial quality surveillance in myocardial infarction: from bench to bedside. Ageing Research Reviews 66:101250.

[19] Wang, Y., Jasper, H., Toan, S., Muid, D., Chang, X., Zhou, H., 2021. Mitophagy coordinates the mitochondrial unfolded protein response to attenuate inflammation-mediated myocardial injury. Redox Biology 45:102049.
[20] Chang, X., Lochner, A., Wang, H.H., Wang, S., Zhu, H., Ren, J., et al., 2021. Coronary microvascular injury in myocardial infarction: perception and knowledge for mitochondrial quality control. Theranostics 11(14):6766–6785.
[21] Zhou, H., Toan, S., Zhu, P., Wang, J., Ren, J., Zhang, Y., 2020. DNA-PKcs promotes cardiac ischemia reperfusion injury through mitigating BI-1-governed mitochondrial homeostasis. Basic Research in Cardiology 115(2):11.
[22] Seefeldt, J.M., Lassen, T.R., Hjortbak, M.V., Jespersen, N.R., Kvist, F., Hansen, J., et al., 2021. Cardioprotective effects of empagliflozin after ischemia and reperfusion in rats. Scientific Reports 11(1):9544.
[23] Song, Y., Huang, C., Sin, J., Germano, J.F., Taylor, D.J.R., Thakur, R., et al., 2021. Attenuation of adverse postinfarction left ventricular remodeling with empagliflozin enhances mitochondria-linked cellular energetics and mitochondrial biogenesis. International Journal of Molecular Sciences 23(1).
[24] Ahmed, A.S., Mona, M.M., Abdel-Kareem, M.A., Elsisy, R.A., 2021. SGLT2 inhibitor empagliflozin monotherapy alleviates renal oxidative stress in albino Wistar diabetic rats after myocardial infarction induction. Biomedicine & Pharmacotherapy 139:111624.
[25] Juni, R.P., Al-Shama, R., Kuster, D.W.D., van der Velden, J., Hamer, H.M., Vervloet, M.G., et al., 2021. Empagliflozin restores chronic kidney disease-induced impairment of endothelial regulation of cardiomyocyte relaxation and contraction. Kidney International 99(5):1088–1101.
[26] Wang, J., Zhu, P., Li, R., Ren, J., Zhang, Y., Zhou, H., 2020. Bax inhibitor 1 preserves mitochondrial homeostasis in acute kidney injury through promoting mitochondrial retention of PHB2. Theranostics 10(1):384–397.
[27] Wang, J., Zhou, H., 2020. Mitochondrial quality control mechanisms as molecular targets in cardiac ischemia-reperfusion injury. Acta Pharmaceutica Sinica B 10(10):1866–1879.
[28] Huang, S., Li, Z., Wu, Z., Liu, C., Yu, M., Wen, M., et al., 2021. DDAH2 suppresses RLR-MAVS-mediated innate antiviral immunity by stimulating nitric oxide-activated, Drp1-induced mitochondrial fission. Science Signaling 14(678).
[29] Gutiérrez, T., Qi, H., Yap, M.C., Tahbaz, N., Milburn, L.A., Lucchinetti, E., et al., 2020. The ER chaperone calnexin controls mitochondrial positioning and respiration. Science Signaling 13(638).
[30] Langston, J.W., 2017. The MPTP story. Journal of Parkinson's Disease 7(s1): S11–S19.
[31] Zhao, Y., Wang, C., Hong, X., Miao, J., Liao, Y., Hou, F.F., et al., 2019. Wnt/β-catenin signaling mediates both heart and kidney injury in type 2 cardiorenal syndrome. Kidney International 95(4):815–829.
[32] Deng, T., Wei, Z., Gael, A., Deng, X., Liu, Y., Lai, J., et al., 2020. Higenamine improves cardiac and renal fibrosis in rats with cardiorenal syndrome via ASK1 signaling pathway. Journal of Cardiovascular Pharmacology 75(6): 535–544.
[33] Liu, Y., Liu, Y., Liu, X., Chen, J., Zhang, K., Huang, F., et al., 2015. Apocynin attenuates cardiac injury in type 4 cardiorenal syndrome via suppressing cardiac fibroblast growth factor-2 with oxidative stress inhibition. Journal of American Heart Association 4(7).
[34] Poveda, J., Vázquez-Sánchez, S., Sanz, A.B., Ortiz, A., Ruilope, L.M., Ruiz-Hurtado, G., 2021. TWEAK-Fn14 as a common pathway in the heart and the kidneys in cardiorenal syndrome. The Journal of Pathology 254(1):5–19.
[35] Wu, F., Li, Z., Cai, M., Xi, Y., Xu, Z., Zhang, Z., et al., 2020. Aerobic exercise alleviates oxidative stress-induced apoptosis in kidneys of myocardial infarction mice by inhibiting ALCAT1 and activating FNDC5/Irisin signaling pathway. Free Radical Biology and Medicine, 158171–158180.
[36] Brown, K., Yang, P., Salvador, D., Kulikauskas, R., Ruohola-Baker, H., Robitaille, A.M., et al., 2017. WNT/β-catenin signaling regulates mitochondrial activity to alter the oncogenic potential of melanoma in a PTEN-dependent manner. Oncogene 36(22):3119–3136.
[37] Ziegler, P.K., Bollrath, J., Pallangyo, C.K., Matsutani, T., Canli, Ö., De Oliveira, T., et al., 2018. Mitophagy in intestinal epithelial cells triggers adaptive immunity during tumorigenesis. Cell 174(1):88–101 e16.
[38] Liu, D., Liu, Y., Zheng, X., Liu, N., 2021. c-MYC-induced long noncoding RNA MEG3 aggravates kidney ischemia-reperfusion injury through activating mitophagy by upregulation of RTKN to trigger the Wnt/β-catenin pathway. Cell Death & Disease 12(2):191.
[39] Bernkopf, D.B., Behrens, J., 2018. Feedback regulation of mitochondrial homeostasis via Wnt/β-catenin signaling. Molecular & Cellular Oncology 5(3) e1458015-e1458015.
[40] Patschan, D., Marahrens, B., Jansch, M., Patschan, S., Ritter, O., 2022. Experimental cardiorenal syndrome type 3: what is known so far? Journal of Clinical Medicine and Research 14(1):22–27.
[41] Drubel, K., Marahrens, B., Ritter, O., Patschan, D., 2022. Kidney-related outcome in cardiorenal syndrome type 3. The Internet Journal of Nephrology 2022, 4895434.
[42] Di Lullo, L., Bellasi, A., Russo, D., Cozzolino, M., Ronco, C., 2017. Cardiorenal acute kidney injury: epidemiology, presentation, causes, pathophysiology and treatment. International Journal of Cardiology, 227143–227150.
[43] Vásquez-Trincado, C., García-Carvajal, I., Pennanen, C., Parra, V., Hill, J.A., Rothermel, B.A., et al., 2016. Mitochondrial dynamics, mitophagy and cardiovascular disease. Journal of Physiology 594(3):509–525.
[44] Fox, B.M., Gil, H.W., Kirkbride-Romeo, L., Bagchi, R.A., Wennersten, S.A., Haefner, K.R., et al., 2019. Metabolomics assessment reveals oxidative stress and altered energy production in the heart after ischemic acute kidney injury in mice. Kidney International 95(3):590–610.
[45] Caio-Silva, W., da Silva Dias, D., Junho, C.V.C., Panico, K., Neres-Santos, R.S., Pelegrino, M.T., et al., 2020. Characterization of the oxidative stress in renal ischemia/reperfusion-induced cardiorenal syndrome type 3. BioMed Research International 2020:1605358.
[46] Junho, C.V.C., González-Lafuente, L., Navarro-García, J.A., Rodríguez-Sánchez, E., Carneiro-Ramos, M.S., Ruiz-Hurtado, G., 2022. Unilateral acute renal ischemia-reperfusion injury induces cardiac dysfunction through intracellular calcium mishandling. International Journal of Molecular Sciences 23(4).
[47] Yang, K.C., Bonini, M.G., Dudley Jr., S.C., 2014. Mitochondria and arrhythmias. Free Radical Biology and Medicine, 71351–71361.
[48] Trentin-Sonoda, M., Fratoni, F.M., da Cruz Junho, C.V., Silva, W.C., Panico, K., Carneiro-Ramos, M.S., 2019. Caspase-1 as molecular key in cardiac remodeling during cardiorenal syndrome type 3 in the murine model. Current Molecular Medicine 20(1):72–78.
[49] Kolijn, D., Pabel, S., Tian, Y., Lódi, M., Herwig, M., Carrizzo, A., et al., 2021. Empagliflozin improves endothelial and cardiomyocyte function in human heart failure with preserved ejection fraction via reduced pro-inflammatory-oxidative pathways and protein kinase Gα oxidation. Cardiovascular Research 117(2): 495–507.
[50] Liu, H., Sridhar, V.S., Montemayor, D., Lovblom, L.E., Lytvyn, Y., Ye, H., et al., 2021. Changes in plasma and urine metabolites associated with empagliflozin in patients with type 1 diabetes. Diabetes, Obesity and Metabolism 23(11): 2466–2475.
[51] Ma, Y., Kan, C., Qiu, H., Liu, Y., Hou, N., Han, F., et al., 2021. Transcriptomic analysis reveals the protective effects of empagliflozin on lipid metabolism in nonalcoholic fatty liver disease. Frontiers in Pharmacology 12, 793586.
[52] Tian, G., Yu, Y., Deng, H., Yang, L., Shi, X., Yu, B., 2021. Empagliflozin alleviates ethanol-induced cardiomyocyte injury through inhibition of mitochondrial apoptosis via a SIRT1/PTEN/Akt pathway. Clinical and Experimental Pharmacology and Physiology 48(6):837–845.
[53] Ala, M., Khoshdel, M.R.F., Dehpour, A.R., 2022. Empagliflozin enhances autophagy, mitochondrial biogenesis, and antioxidant defense and ameliorates

renal ischemia/reperfusion in nondiabetic rats. Oxidative Medicine and Cellular Longevity 2022:1197061.

[54] Tan, Y., Yu, K., Liang, L., Liu, Y., Song, F., Ge, Q., et al., 2021. Sodium-glucose Co-transporter 2 inhibition with empagliflozin improves cardiac function after cardiac arrest in rats by enhancing mitochondrial energy metabolism. Frontiers in Pharmacology 12:758080.

[55] Zhou, H., Wang, S., Zhu, P., Hu, S., Chen, Y., Ren, J., 2018. Empagliflozin rescues diabetic myocardial microvascular injury via AMPK-mediated inhibition of mitochondrial fission. Redox Biology, 15335—15346.

[56] Cai, C., Guo, Z., Chang, X., Li, Z., Wu, F., He, J., et al., 2022. Empagliflozin attenuates cardiac microvascular ischemia/reperfusion through activating the AMPKα1/ULK1/FUNDC1/mitophagy pathway. Redox Biology 52:102288.

[57] Mizuno, M., Kuno, A., Yano, T., Miki, T., Oshima, H., Sato, T., et al., 2018. Empagliflozin normalizes the size and number of mitochondria and prevents reduction in mitochondrial size after myocardial infarction in diabetic hearts. Physiological reports 6(12) e13741-e13741.

[58] Philipson, B.I., O'Connor, R.S., May, M.J., June, C.H., Albelda, S.M., Milone, M.C., 2020. 4-1BB costimulation promotes CAR T cell survival through noncanonical NF-κB signaling. Science Signaling 13(625).

[59] Zhou, H., Du, W., Li, Y., Shi, C., Hu, N., Ma, S., et al., 2018. Effects of melatonin on fatty liver disease: the role of NR4A1/DNA-PKcs/p53 pathway, mitochondrial fission, and mitophagy. Journal of Pineal Research 64(1).

[60] Selvarajah, B., Azuelos, I., Anastasiou, D., Chambers, R.C., 2021. Fibrometabolism-An emerging therapeutic frontier in pulmonary fibrosis. Science Signaling 14(697).

[61] Shen, Y., Wang, X., Liu, Y., Singhal, M., Gürkaşlar, C., Valls, A.F., et al., 2021. STAT3-YAP/TAZ signaling in endothelial cells promotes tumor angiogenesis. Science Signaling 14(712):eabj8393.

[62] Cai, Y., Kim, D.J., Takahashi, T., Broadhurst, D.I., Yan, H., Ma, S., et al., 2021. Kynurenic acid may underlie sex-specific immune responses to COVID-19. Science Signaling 14(690).

[63] Apel, F., Andreeva, L., Knackstedt, L.S., Streeck, R., Frese, C.K., Goosmann, C., et al., 2021. The cytosolic DNA sensor cGAS recognizes neutrophil extracellular traps. Science Signaling 14(673).

[64] Zhou, H., Hu, S., Jin, Q., Shi, C., Zhang, Y., Zhu, P., et al., 2017. Mff-dependent mitochondrial fission contributes to the pathogenesis of cardiac microvasculature ischemia/reperfusion injury via induction of mROS-mediated cardiolipin oxidation and HK2/VDAC1 disassociation-involved mPTP opening. Journal of American Heart Association 6(3).

[65] Sriram, G., Milling, L.E., Chen, J.K., Kong, Y.W., Joughin, B.A., Abraham, W., et al., 2021. The injury response to DNA damage in live tumor cells promotes antitumor immunity. Science Signaling 14(705):eabc4764.

[66] Jiang, X., Prabhakar, A., Van der Voorn, S.M., Ghatpande, P., Celona, B., Venkataramanan, S., et al., 2021. Control of ribosomal protein synthesis by the Microprocessor complex. Science Signaling 14(671).

